# THE COMPRESSIBLE INVISCID VORTEX FLOW
# OF A SHARP EDGE DELTA WING[(*)]

## J.M.A. Longo

DLR - Braunschweig
Institut of Design Aerodynamic
Lilienthalplatz 7,D-38108 Braunschweig, Fed. Rep. Germany
(Telephon +49/531-295 2833 , Telefax +49/531-295 2320)

## Abstract

An analysis is presented on the compressible inviscid vortex flow over three delta wings with sharp leading edges with leading edge sweep angles $\varphi = 60°$ , $70°$ and $76°$ using numerical solutions of the Euler equations. Presentations of results are given for Mach numbers ranging from $M_\infty = 0.1$ to $0.8$ and for angles of attack up to the onset of vortex breakdown. The paper focusses the attention on the effects of the vortex flow on the flow field of a delta wing. The occurence of shock waves of two types: cross-flow and terminating (or rear) shocks in the vortical flow fields are investigated; the possibility of shock induced vortex breakdown and the effects of compressibility on the rapid performance degradation of delta wings after vortex bursting are studied in detail. Moreover, the changes on flow kinematic within the vortex core due to the close presence of the wing are also studied.

## 1. Introduction

The vortical flow field generated around sharp edged delta wings at high angle of attack has been the subject of numerous research activities in the last thirty years. Most of the existing investigations, however, were carried out at subsonic or supersonic conditions, as is shown from the excellent comprehensive reviews published by Hoeijmakers[1] and Newsome et al.[2]. Experimental investigations at transonic free stream Mach numbers[3],[4] have shown a complicated flow field with cross flow shocks, terminating or rear shocks and leading edge shocks partially embedded in the flow field which is generated by the leading edge vortices. The influence of the shocks on the breakdown of the vortices and on the degradation of the aerodynamics performances of the delta wing after vortex bursting is still unknown. Similarly, other questions related to the physics of the compressible flow within the vortex core remain until now unanswered. Although Navier-Stokes solutions were shown to be qualitative and also quantitative more accurate than Euler results[5],[6] the improvements of the solutiion are restricted to secondary effects. Today numerical methods based on the solution the Euler equations have

reached enough maturity to be used to describe essential flow features like the production vortex lift, the interaction between shock and vortices and the prediction of vortex break down. The interested reader is referred to the many paper published during recent years[6] - [16]. To contribute to a better understanding of the compressible vortex flow fields of sharp edged delta wings, a systematic study using the DLR CEVCATS Euler code is reported in the present work. Three delta wings with sharp leading edges, with sweep angles of $\varphi = 60°$ , $70°$ and $76°$ are studied for $0.1 \le M_\infty \le 0.8$ for angles of attack up to vortex breakdown.

## 2. Numerical experiment setup

### 2.1 Computer code

The simulations of the flow field are done by means of steady-state solutions of the Euler equations, representing conservation of mass, momentum and energy. The numerical solutions are computed with the DLR CEVCATS Euler code. The description of the basic solution method for the numerical algorithm are given in[17]-[19]. The computational algorithm employs a finite-volume spatial discretization, in which the discrete values of the flow quantities are located at the vertices of the mesh cell. Artificial dissipative terms (also known as artificial viscosity) based on the work of Jameson et al.[20] are added to the governing discrete equations. The magnitudes of these terms are depending on the pressure gradients in the flow and damping coefficients specified by the user. The system of ordinary differential equations which is obtained by the discretization in space is advanced in time with a five stage Runge-Kutta scheme. Three methods are used to accelerate convergence to steady state: local time stepping, implicit smoothing of the residuals and a multigrid method. The code allows multiblock decomposition of the computational domain and it is therefore grid topology independent. The required computer time per each angle of attack and or Mach number in presence of vortex breakdown is 30 minutes on a CRAY-YMP computer. This time includes the time required to read and write data files and the time required to perform the calculations.

## 2.2 Configurations and grid

In the present study three delta wings with sharp leading edges and leading edge sweep angles of $\varphi = 60°$, $70°$ and $76°$ and symmetric wing profiles (Fig.1-a) are numerically tested. The physical domain is discretized by means of a four block H-H topology grid consisting on 450000 points (Fig.1-b). This topology structure offers high flexibility to geometrical changes on the configuration without altering the whole domain. On each block the mesh is generated in three main steps[16]: first a 3-D body fitted grid is generated via transfinite interpolation; then a 2-D elliptic solver is applied on each block face and finally a 3-D elliptic solver is used to smooth the grid inside each block enforcing orthogonality of the grid lines at block boundaries. The outer boundaries of the computational domain extend approximately 6 wing root chords in all directions. The clustering of grid lines in direction normal to the surface of the configuration has a minimum spacing for the first mesh layer of $\leq 10^{-3}$ chord lengths. Additionally, minimum values of the dissipation coefficients are used to yield solutions practically not contaminated by artificial dissipation.



**(a)**

**(b)**

Fig. 1    Numerical experiment set-up
(a) configurations - (b) grid structure

## 2.3 Computation of vortex bursting

The governing equations and computational algorithms used for this investigation were formulated to achieve steady state solutions. The criterion used to determine when the solution converged to its steady state is the residual convergence of the continuity equation, namely the $L_2$-Norm. Converged solutions are assumed once the $L_2$-Norm drops at least through three orders of magnitude. A different time interval is used in each cell to accelerate the convergence to steady state and hence the discrete equations are not solved in a time accurate fashion. Once the vortex bursts, the flow field induced by the vortex becomes unsteady. At the location of the vortex bursting and downstream this point along the vortex axis, the numerical solution does not converge to a steady state but it exhibits an oscillatory motion of low frequency. At the same time the velocity profile of the axial component of the core flow changes its character from jet- type to wake type. However, it was found that for flow conditions corresponding to vortex bursting the solutions are not diverging. Instead, they have converged to results which are globally stationary but locally unsteady. Furthermore, the comparison of these solutions with experimental data[16] shows good agreement. In the present work vortex breakdown is defined as the place where the second derivative of the axial component of the core flow with respect to the core radius is zero (i.e. $\partial^2 u / \partial r^2 = 0$). This criterium for the determination of the place where the vortex bursts has been succesfully applied in previous experimental and numerical studies of vortex breakdown[21] and[16].

### 3. Results and Discussion

#### 3.1 Forces and pitching moments

Aerodynamics forces and pitching moments for the three delta wings for two free stream Mach numbers, 0.4 and 0.8 are shown in Fig.2. It is shown that the effect of the the Mach number on the total forces and pitching moment is larger for delta wings with small sweep. Also, as the wing leading edge sweep angle increases, the slope of the lift curves decreases due to the reduction of the wing aspect ratio, but the value of the maximum lift coefficient and the corresponding angle of attack increases. For the wing with $\varphi = 76°$, lift and drag curves, maximum lift coefficients and corresponding angles of attack are similar for both Mach numbers. Also, in both cases the maximum lift is reached at the angle of attack where the vortex bursts at the wing trailing edge. Since the center of pressure of the wing moves downstream with increasing Mach number, the pitching moment is more negative (nose down) for larger values of the free stream Mach number. The $\varphi = 70°$ wing shows not only changes on pitching moment, but also the
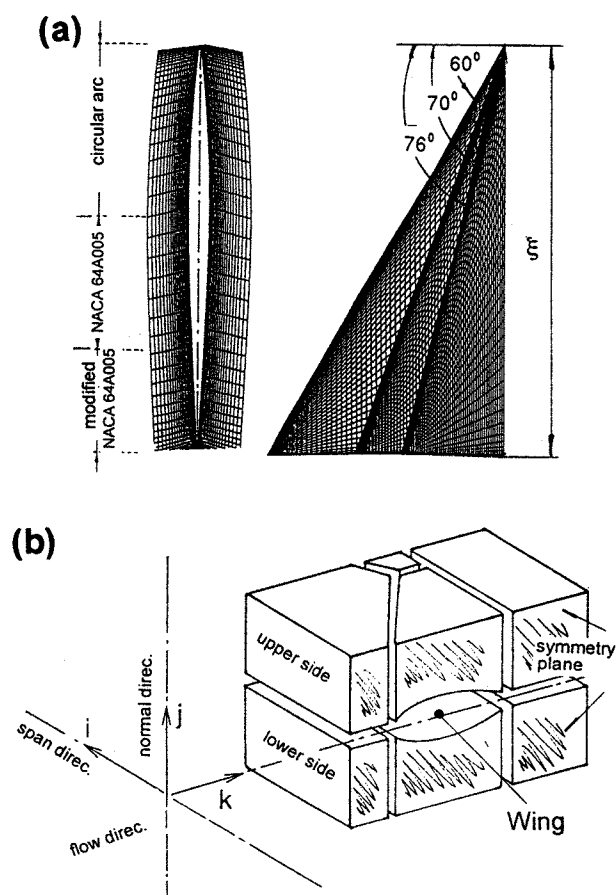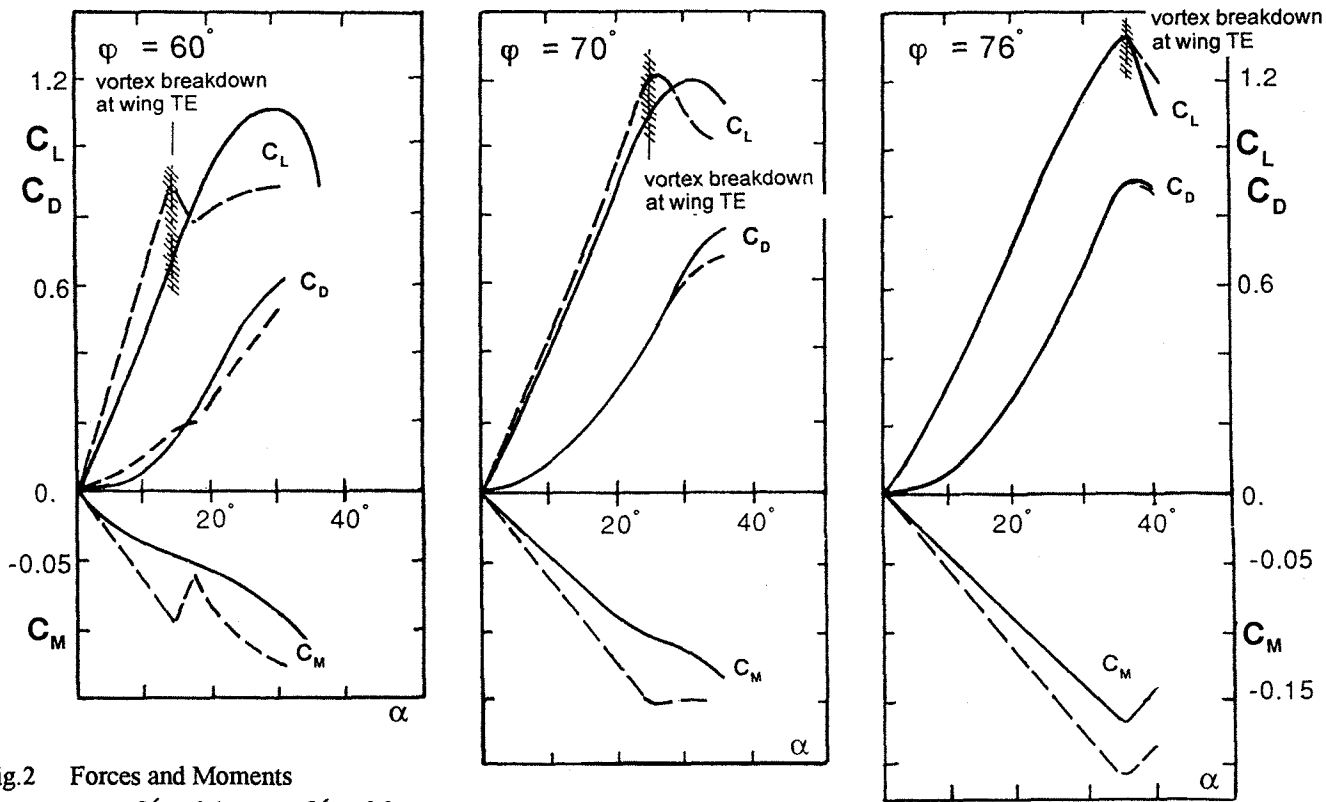
Fig.2   Forces and Moments
------- $\mathcal{M}_\infty = 0.4$, -------- $\mathcal{M}_\infty = 0.8$

lift slope is larger for the higher Mach number. The maximum lift coefficients are similar for both Mach numbers but it is produced at a lower value of the angle of attack for the higher free stream Mach. However, the onset of the vortex breakdown at the wing trailing edge is not influenced by the change in free stream Mach number. Finally, the wing with $\phi = 60°$ exhibits the largest Mach number effects. For low and medium angles of attack the lift slope increases as the Mach number increases. The onset of the vortex breakdown at the trailing edge take place at approximately the same angle of attack for both free stream Mach numbers ($\propto \approx 15°$), but the aerodynamic behavior at larger angles is totally different. On the one hand, for the low Mach number case the lift continues to increase at the same rate and later decays smoothly. Maximum lift for $M_\infty = 0.4$ is reached once the leading edge vortex is totally bursted above the wing (see the iso-$C_P$ of Fig.3). On the other hand, for the high Mach number the lift slope shows first a sudden drop followed by a flat recovery. This behavior for the $M_\infty = 0.8$ case is due to the fast upstream shift of the vortex bursting location with increasing angle of attack, as is shown in Fig.4. This faster upstream progression of the breakdown for the wing $\phi = 60°$ produces a large loss of vortex lift. Since this phenomenon starts at a relative small incidence, the loss of vortex lift can not be compensated by the pressure increase along the lower surface of the wing.

As the angle of attack increases, the loss of lift on the lee side of the wing becomes partially compensated by a gain of lift from the windward side, producing a flat recovery of the lift curve. The induced drag and pitching moment curves show a similar behavior.

## 3.2 Shock-vortex interaction

Figure 5 shows iso-$C_P$ lines for the $\phi = 60°$ wing at $M_\infty = 0.8$ and angles of attack where the slope of the lift curve experiences the major changes. Also the figure shows some streamlines with the corresponding values of the local Mach numbers to recognize possible occurrence of shock waves. Supersonic and subsonic flow areas are distinguished by means of white and grey colors, respectively. At $\propto = 14°$ (short before the begining of the vortex breakdown at the wing trailing edge), the flow underneath the leading edge vortex is fully supersonic and also there is a small sonic area close to the symmetry plane. There are no terminating or rear shocks above the wing, but a small strong cross-flow shock is developed close to the wing trailing edge. At higher angles of attack this cross-flow shock moves upstream together with the point of the vortex bursting. Downstream of the vortex bursting the flow remains supersonic but it is oriented towards the wing trailing edge and hence, there a terminating shock compresses
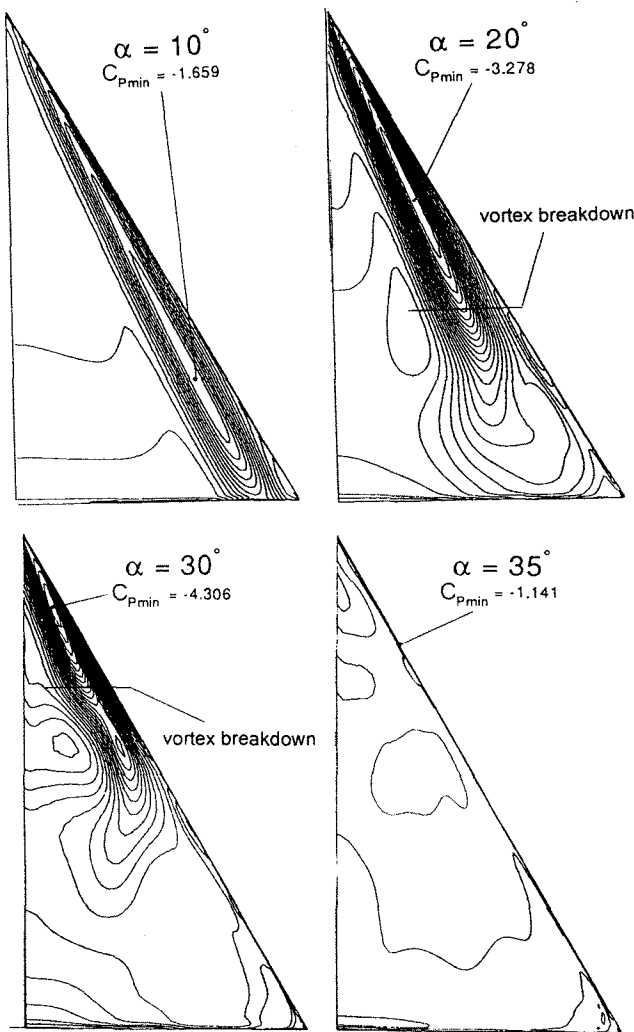
$\alpha = 10°$  $C_{Pmin} = -1.659$

$\alpha = 20°$  $C_{Pmin} = -3.278$

vortex breakdown

$\alpha = 30°$  $C_{Pmin} = -4.306$

vortex breakdown

$\alpha = 35°$  $C_{Pmin} = -1.141$

Fig.3    Iso-$C_P$ - Wing $\varphi = 60°$ - $M_\infty = 0.4$
*Effect of the Mach number on the bursting progression*



$\varphi = 60°$
$M_\infty = 0.4$ ———
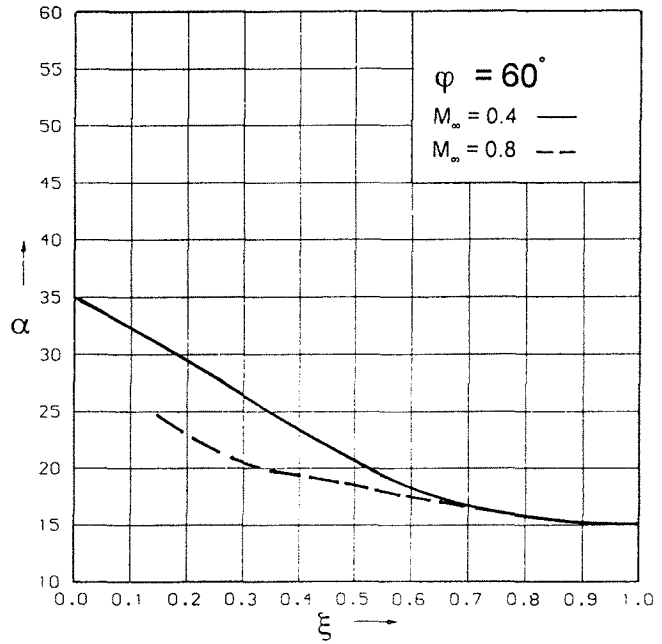$M_\infty = 0.8$ — —

Fig.4    Vortex Bursting - Wing $\varphi = 60°$
*Effect of the Mach number on the bursting progression*

the flow to the free stream pressure. The upstream shifting of the vortex breakdown together with the cross-flow shock continues as the angle of attack increases. While the terminating shock appears after the breakdown of the vortex, the role of the cross-flow shock on the onset of the vortex breakdown and its upstream shifting is not clear. To clarify this aspect, Fig.6, 7 and 8 display a similar analysis for the wing with $\varphi = 70°$. The onset of vortex breakdown at the wing trailing edge for $0.4 \leq M_\infty \leq 0.8$ begins at approximately the same angle of attack ($\alpha \cong 25°$) but the upstream shifting of the vortex bursting is faster for free stream Mach numbers larger than 0.4 (see Fig.6). In Fig.7 the



$\alpha = 14°$

M = 1.

$C_{Pmin} = -1.754$

M = 1.76
M = 0.83

cross-flow shock

$\alpha = 17°$

M = 1.02
$C_{Pmin} = -1.834$
M = 2.15
M = 1.25
M = 0.89
cross-flow shock
M = 1.24

terminating shock

$C_{Pmin} = -1.579$
$\alpha = 20°$
M = 1.2
M = 0.9
cross-flow shock
M = 1.05
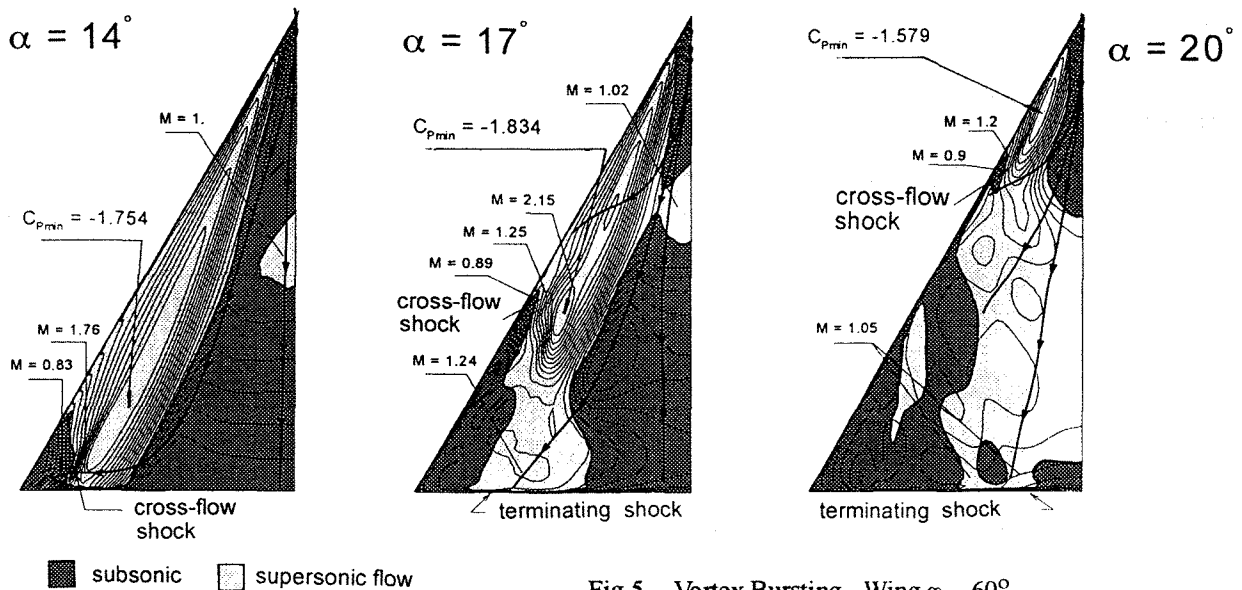
terminating shock

■ subsonic    □ supersonic flow

Fig.5    Vortex Bursting - Wing $\varphi = 60°$
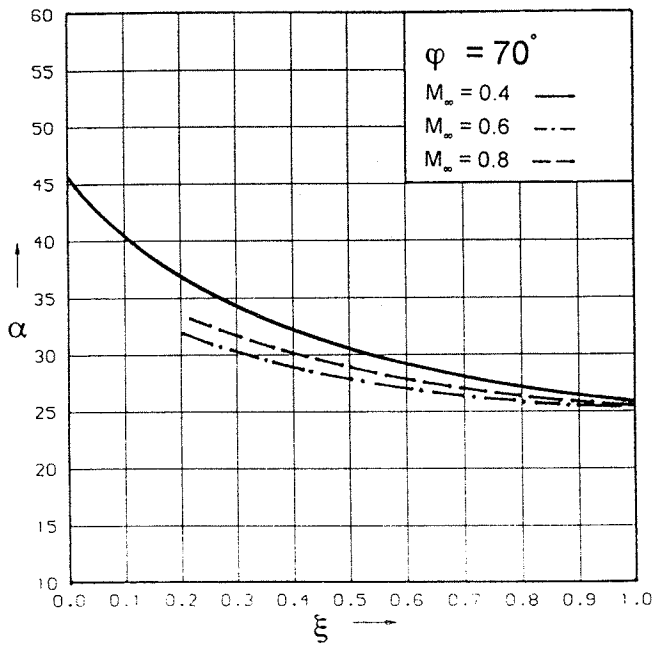*Effect of the Mach number on the bursting progression*

793

Fig.6    Vortex Bursting - Wing $\varphi = 70°$
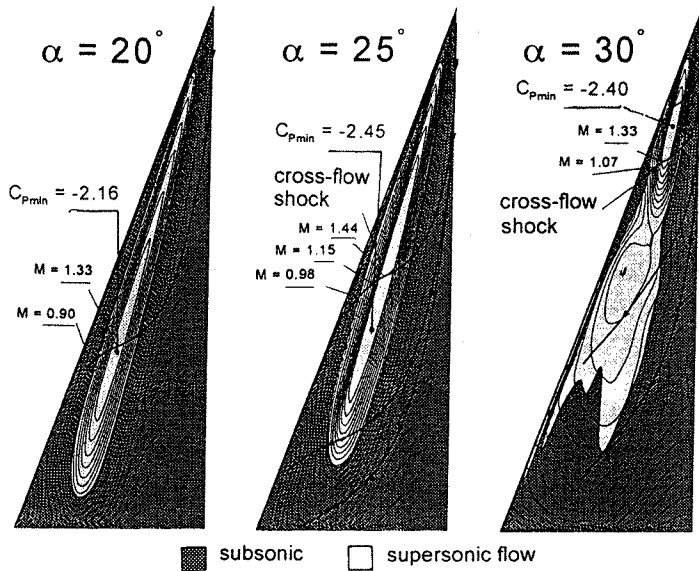*Effect of the Mach number on the bursting progression*



Fig.7    Iso-$C_P$ - Wing $\varphi = 70°$ - $M_\infty= 0.6$
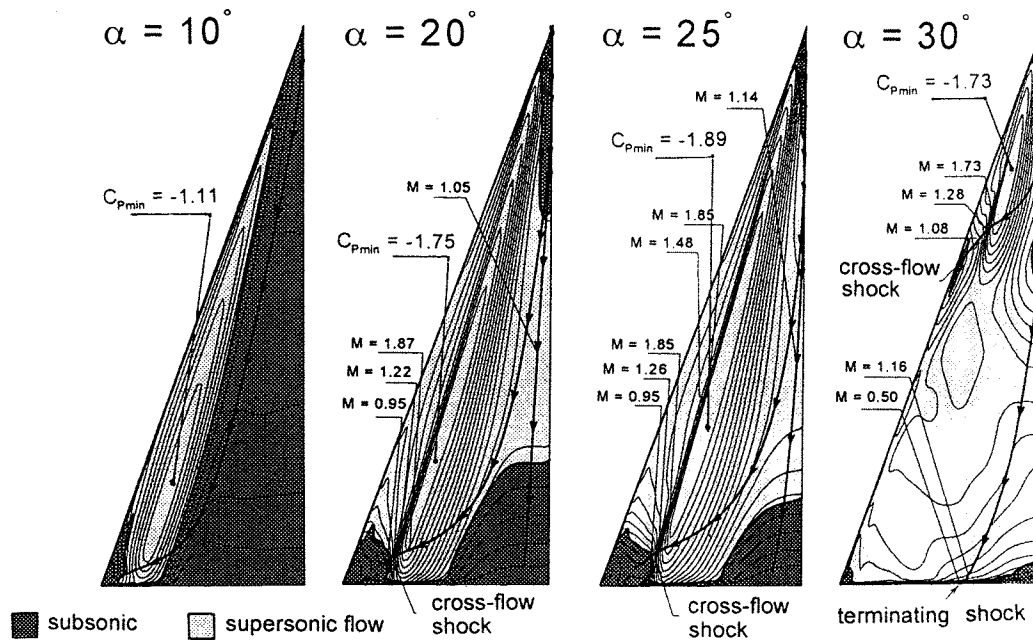*Effect of the angle of attack on the transonic vortex flow*



Fig.8    Iso-$C_P$ - Wing $\varphi = 70°$ - $M_\infty= 0.8$
*Effect of the angle of attack on the transonic vortex flow*

pressure fields for $M_\infty= 0.6$ indicate that the flow close to the wing trailing edge is fully subsonic for the angle of attack for the onset of vortex bursting at wing trailing edge ($\propto \cong 25°$) . Moreover, only a weak cross- flow shock is present in the field at x/c $\cong 0.5$ , underneath the leading edge vortex. By increasing the angle of attack the vortex breakdown shifts upstream as does the cross-flow shock. Close to the wing trailing edge the flow remains subsonic.

Supersonic flow at the wing surface is only observed underneath the vortex core and also downstream the location of vortex breakdown. Finally, Fig.8 shows the corresponding solutions for $M_\infty= 0.8$ . For $\propto = 10°$ the flow underneath the leading edge vortex is already supersonic. At $\propto = 20°$ the supersonic region extends towards the symmetry plane. Furthermore, a strong cross-flow shock develops underneath the primary vortex. At the initiation of the burst-

794

ing process the flow above the wing is almost fully supersonic. A strong cross-flow shock lies underneath the leading edge vortex and extends up to the station x/c ≈ 0.3 . Once the location of vortex breakdown passes the trailing edge in direction to the wing apex ($\alpha > 25°$), a terminating shock develops at the trailing edge of the wing. Although the cross-flow shock for $M_\infty= 0.8$ is stronger than the corresponding shock for the $M_\infty= 0.6$ case, the upstream progression of the vortex bursting is faster for $M_\infty= 0.6$ than for the $M_\infty= 0.8$ case (see Fig.6). Figure 9 shows flow characteristics for the wing $\phi = 70°$ at $\alpha = 20°$, for the crosswise plane $\xi = 0.6$ and for different Mach numbers. The iso-lines of the local Mach number (Fig.9-a) indicate the flow inside the vortex core reaches values almost two times larger than the free stream Mach number. The core flow is already supersonic for $M_\infty> 0.5$ . As the free stream Mach number increases, the region of high-speed core flow grows from the vortex core in radial direction inducing supersonic flow also near the symmetry plane. It turns out that the flow on the upper surface of the wing is mainly oriented in crosswise direction towards the leading edge of the wing. Only close to the symmetry plane remains a small area with streamwise directed flow, where terminating shocks may develop (see also Fig.8). However, in the present investigation occurence of terminating shocks was observed always after vortex breakdown.

### 3.3 Core flow effects on near field wing

Close to the vortex axis Fig.9-a shows that there are two relative maximums of local Mach of about the same magnitude, one above the vortex axis and one below close to the wing surface. Considering a local Mach number defined only with the spanwise component of the velocity (Fig.9-b), here denoted as $M_{cross}$, the iso-Mach lines still exhibit two relative maximum but now of different magnitude. Above the vortex axis, $M_{cross}$ is of the same order of $M_\infty$ and hence it is a factor two smaller than the corresponding local Mach number at this location. Below the vortex axis $M_{cross}$ is of the same order of the local Mach number. The flow between the vortex axis and the wing surface may be considered similar to a convergent-divergent channel flow where the subsonic core flow accelerates to supersonic speed. Hence a cross-flow shock forms underneath the vortex axis already for relative low free stream Mach numbers. Figure 10 shows the $C_P$ and $M_{cross}$ distribution along generic wall stream lines which cross over the wing station $\xi = 0.6$ at the position of the maximum suction peak of pressure for different free stream Mach numbers. Close to the wing apex the flow is oriented in streamwise direction only. There, the largest suction pressure corresponds to the lowest free stream Mach number. As the streamline is going into the channel, the spanwise component of the Mach number $M_{cross}$ increases. For
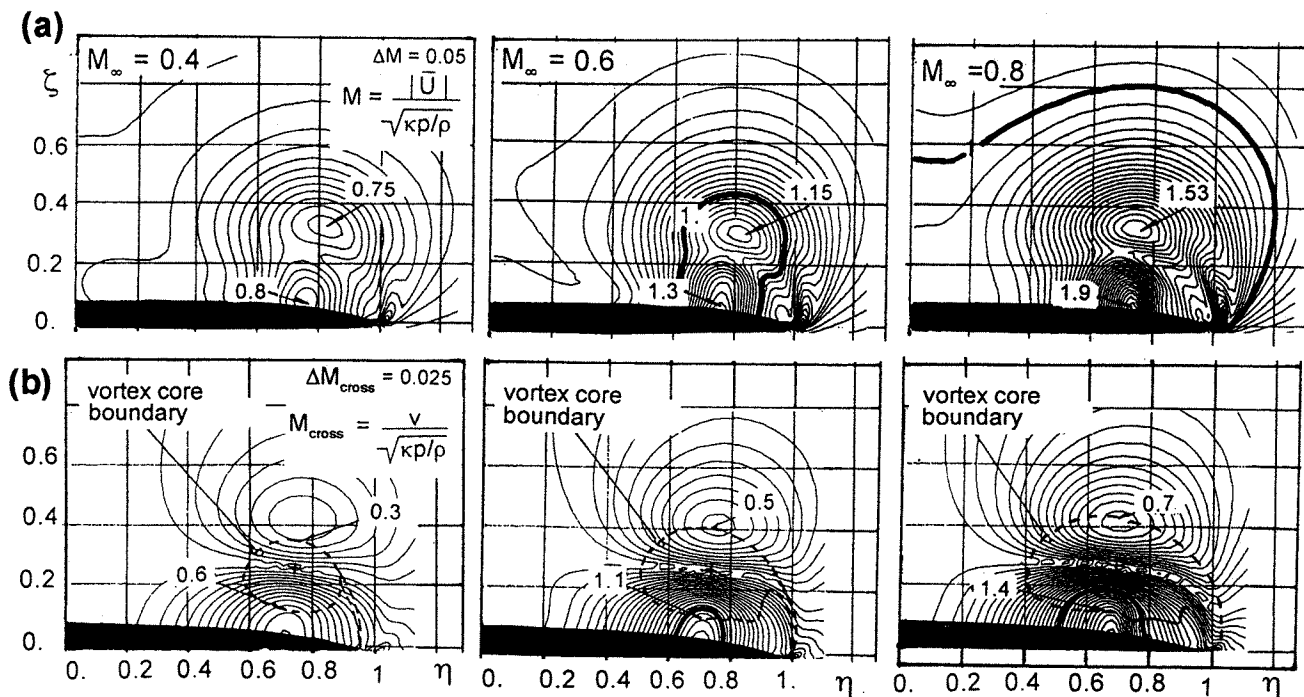


Fig.9    Iso-Mach lines - Wing $\phi = 70°$ - $\alpha = 20°$
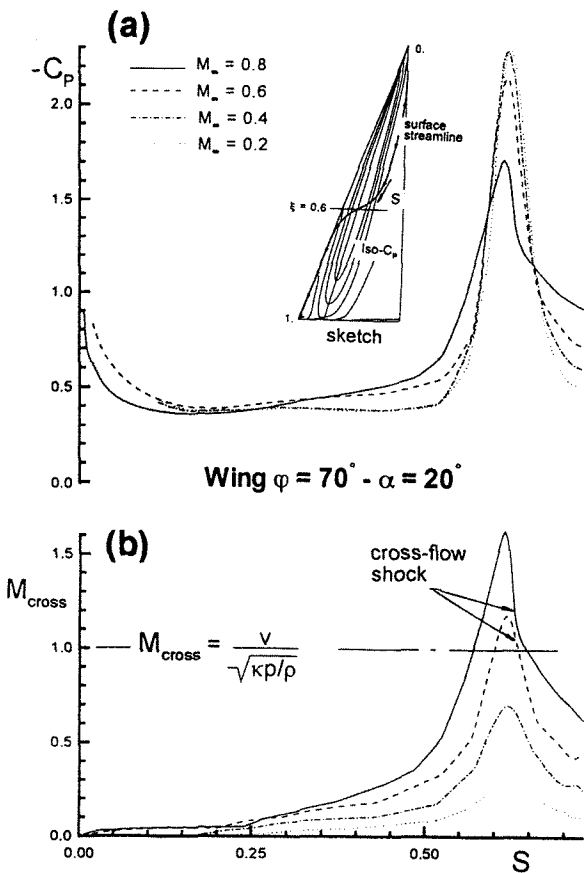         (a)*local Mach* - (b)*local Mach in spanwise direction*

**Fig.10** Flow characteristic along surface stream lines
*(a) Iso-C_p - (b) local Mach*

larger values of the free stream Mach number is $M_{cross}$ supersonic inside the channel. Hence a cross-flow shock develops to compress the supersonic flow to subsonic at the exit of the channel. The location of this cross-flow shock is slightly outboard of the vortex axis. Corresponding with this Mach number behavior, the suction pressure shortly before the entrance of the channel increases but once the flow becomes supersonic, the suction pressure reduces. This effect is also observable during experiments[22]. Figure 11 shows the types of flow experimentally found on sharp leading edged delta wings[23] and the boundaries between them, displayed in a plane of $M_N$ and $\propto_N$, where $M_N$ is the Mach number component normal to the wing leading edge defined as $M_N = M_\infty(1 - \sin^2\varphi \cos^2\propto)^{0.5}$. The present investigation shows that cross-flow shocks already develop for $M_N \approx 0.4$. This new location found for the boundary for the ocurrence of embeded shocks beneath vortices is shaded on Fig.11 in gray. The experimental works reported in[3],[4] are in agreement with this new boundary.

### 3.4 Wing effects on near field core flow

Figure 12 shows flow pictures of lines of constant velocities for the wing $\varphi = 70°$ for $\propto = 20°$ and two Mach num-

bers $M_\infty = 0.1$ and 0.8. They are referred to a coordinate system oriented with the vortex axis, and plotted in a plane perpendicular to the vortex axis, which cross the point $\xi = 0.6$ at the symmetry plane of the wing. In this coordinate system, u is the component of the velocity along the vortex axis (axial velocity), v is the component of the velocity in transversal direction and w is the component of the velocity normal to the vortex axis. At the vortex axis the axial velocity exhibits a maximum, while the other two components vanish. However the flow motion is not rotationally symmetric also in this reference system aligned with the vortex axis. Comparing the magnitude of the normal component with the magnitude of the transversal component of the velocity, it comes out that the maximum values of the v component of the flow motion are almost two times larger than the maximum values of the w component due to the channel formed between the vortex core and the wing surface. As proposed by Batchelor[24], the link between the swirl velocity and the axial velocity components of the motion is provided basically by the pressure. The radial pressure gradient balances the centrifugal force and any change in the swirl velocity, with distance downstream along the
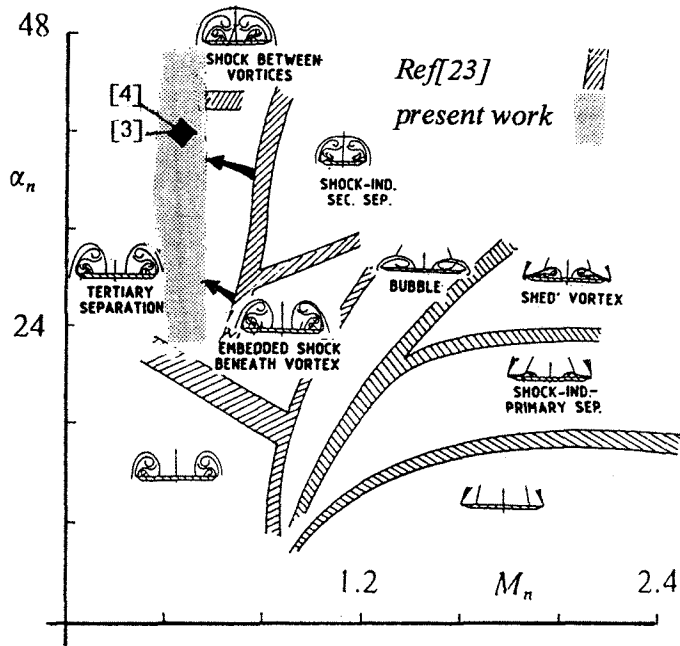


**Fig.11** Flow boundaries for sharp edged delta wings[23]

vortex axis produces an axial pressure gradient and consequently a change on the axial velocity. For inviscid rotational symmetric flows this mechanism of velocity transfer between swirl and axial components leads to a maximum of total velocity at the vortex axis. However, due to the lack of rotational symmetry in case where a solid wall is close to the vortex core, the total velocity of the flow motion ex
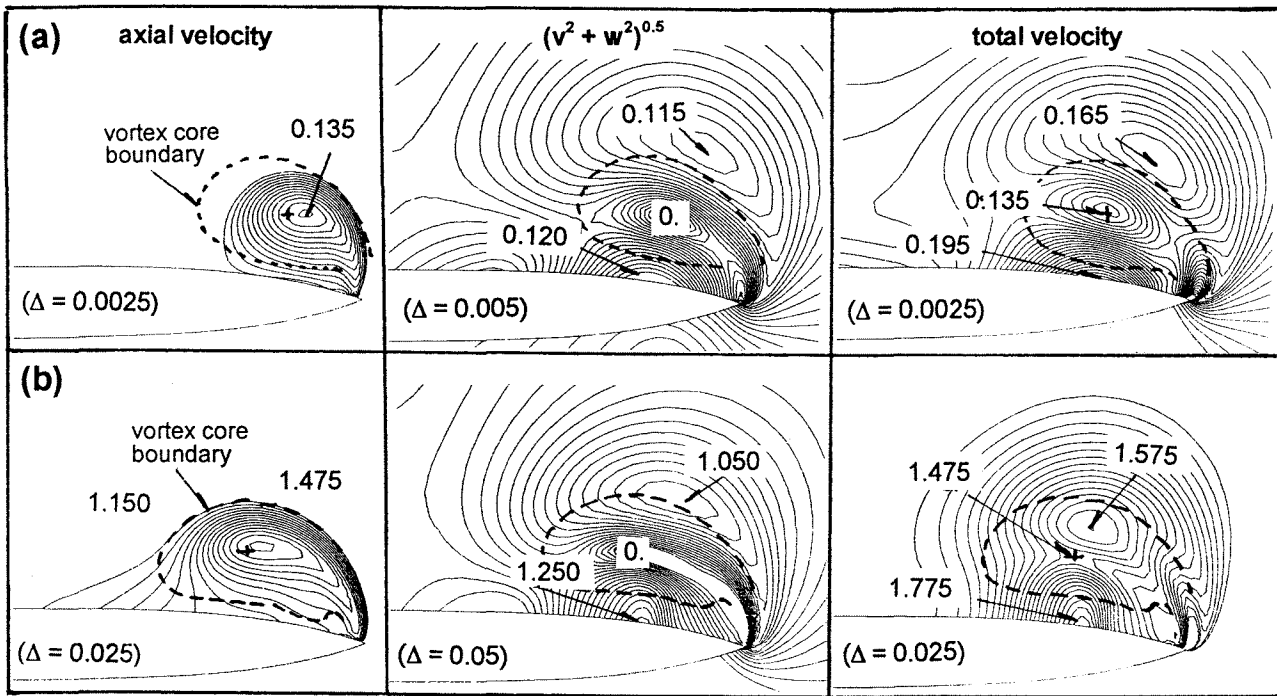
Fig.12 Iso-velocity lines - Wing $\varphi = 70°$ - $\propto = 20°$
(a)$\mathcal{M}_\infty = 0.1$ - (b)$\mathcal{M}_\infty = 0.8$

hibits a relative minimum at the vortex axis. Relative maximums of the total velocity are above and below the vortex axis. This deficit of the total velocity at the vortex axis is also observed in experiments[25]. While in real viscous flow the viscosity carried by the shear layer is another source which enlarges this effect, in the inviscid numerical simulation the discretization error may also enlarge this deficit on velocity, as was already shown in[10]. The present simulations exhibit approximately a 15% deficit on total velocity at the vortex axis, which is more or less free

stream Mach number independent. . The kinematic conditions necessary for a rotationally symmetric flow motion is a zero radial component of the velocity ($V_r = 0$) . This implies that a flow picture for the iso-velocity lines ($v^2 + w^2$)$^{1/2}$ should by concentric circles with the vortex axis at the center. However, Fig.12 reveals that the inviscid vortex flow motion of a delta wing is not free of radial velocities. On the contrary, within the vortex core there are strong radial velocities, which are source of vorticity production as was already shown in[26]. In Fig.13 are shown lines of constant vorticity within the vortex core. They are referred
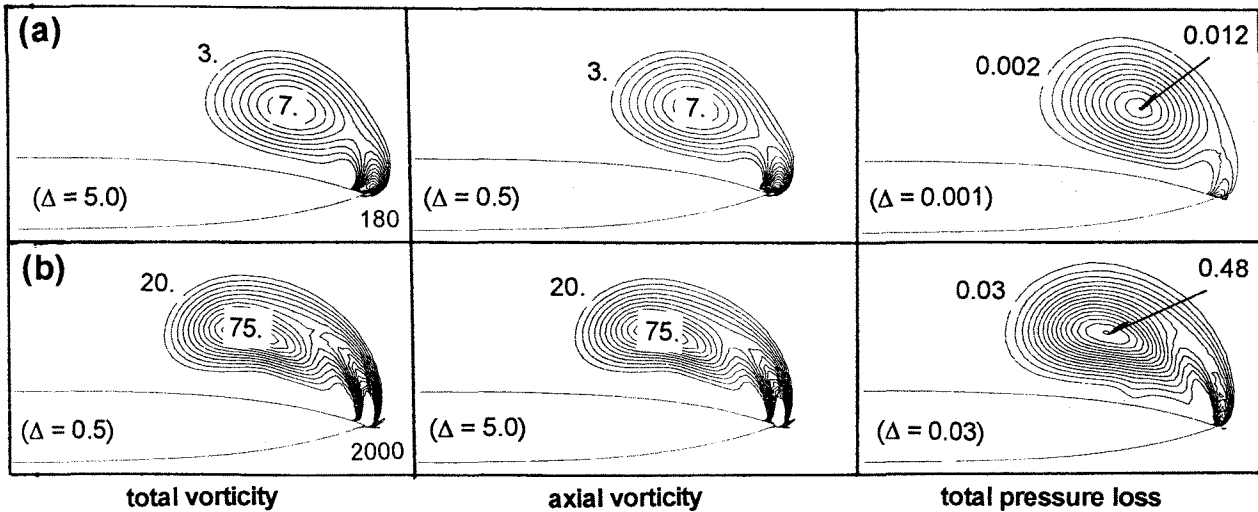


Fig.13 Vorticity and total pressure loss - Wing $\varphi = 70°$
(a)$\mathcal{M}_\infty = 0.1$ - (b)$\mathcal{M}_\infty = 0.8$

797

to the same coordinate system used for the iso-velocity lines of Fig.12, i.e. a coordinate system oriented with the vortex axis and as like as for Fig.12, they are plotted in a plane perpendicular to the vortex axis which cross the point $\xi = 0.6$ a the symmetry plane of the wing. Figure 13 shows that the main source of vorticity production in the field is the leading edge of the wing. There the magnitude of the vorticity is about 27 times larger than at the vortex axis. At the vortex core the axial component of the vorticity is almost the total amount of vorticity generated within the core. The other two components are almost five times smaller and they act only at the outer boundary of the vortex core. Recalling the definition of the axial vorticity component $\gamma_x$, where $\gamma_x = \partial v/\partial z - \partial w/\partial y$, it turns out that only in case that $\partial v/\partial z = \partial w/\partial y$ there may be a rotationally symmetric vortex flow motion. For the inviscid vortex flow above a delta wing is $\partial v/\partial z$ about five times larger than $\partial w/\partial y$. The presence of the wing surface on the near field of the vortex core leads to an acceleration of the vortical flow motion in crosswise direction which introduces strong radial velocities. The vortex core deforms under the action of the resulting different centrifugal forces acting at top and bottom. The resulting vortex core shape is rather flat. Regarding that vorticity is simple twice the angular velocity, an aditional and dominant source of vorticity is introduced within the compressible core flow (the first one is the vorticity feeding from the leading edge), via a fully inviscid mechanim, i.e. without to appeal to any kind of viscous forces -real or numeric-. According to Crocco's theorem in 3-D rotational flows positive entropy gradients VS

are generated each time the vorticity vector $\Omega$ is not aligned with the velocity vector V, i.e. $VS \approx \Omega xV$. Furthermore, for calorically perfect gas these entropy changes are equal to the losses of total pressure experienced by the gas. Figure 13 shows that within the inviscid vortex core the vorticity vector is tangent to the vortex axis while according to Fig.12 the velocity vector has a resulting direction towards the wing surface. This misalignment of both vectors leads to entropy production as one can observe from the contours of total pressure loss given in Fig.13-c. The analysis of the components of the cross product $\Omega xV$ (Fig.14) shows that the dominant term is $\gamma_x.v$, i.e. the axial vorticity $\gamma_x$ times the spanwise component of the velocity v. Also, it turns out that the observed deficits on the axial velocity have only a small contribution to the losses of total pressure found within the vortex core. While the above described inviscid mechanism of entropy production is also present on real flow, the distribution of velocities within a viscous core and within an inviscid one should not necessarily match. The shear layer of a viscous flow carries additional losses of total pressure. Nevertheless, correlations between numerical and experimental maximum values of total pressure have shown good agreement[7],[16] at the vortex axis. Finally, Fig.15 shows values of density $\rho$ and total pressure loss $C_{Pt}$ computed at the vortex core. It comes out that the core flow is compressible even for low free stream Mach numbers. However, significant quantitative losses of total pressure occurs for free stream Mach numbers $M_\infty$ >0.2 .
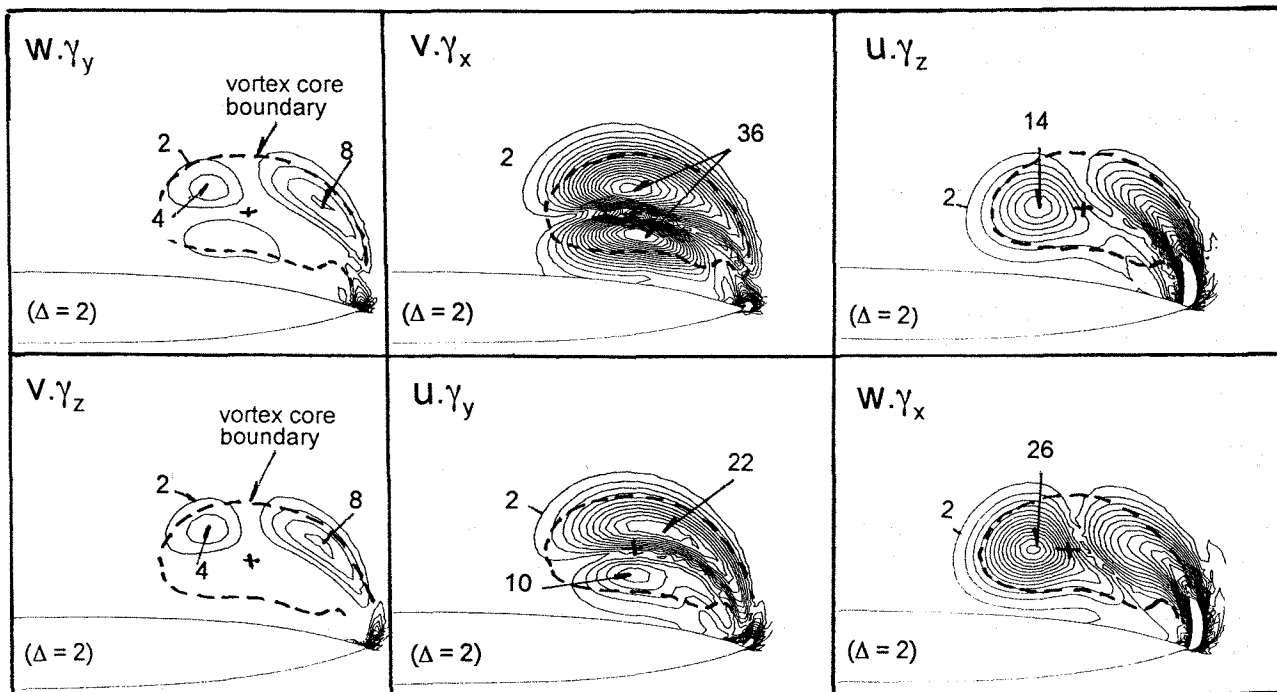


Fig.14 Components of the cross product $\Omega xV$
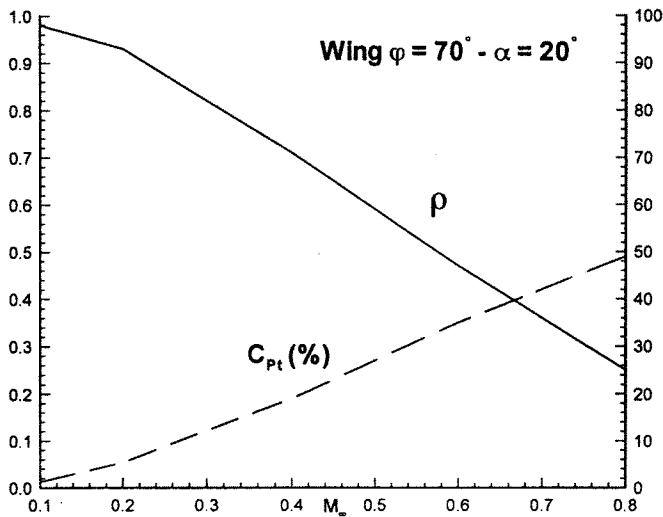(a) $M_\infty = 0.1$ - (b) $M_\infty = 0.8$

**Fig.15** Density and losses of total pressure at vortex axis

## 4. Conclusions

The inviscid compressible leading edge vortex flow of a sharp edge delta wing was studied by means of the numerical solution of the Euler equations. Solutions were obtained for three delta wings with sweep leading edge angles of $\varphi = 60°$, $70°$ and $76°$, for free stream Mach numbers $0.1 \leq M_\infty \leq 0.8$ and for angles of attack up to vortex breakdown.

The present investigation have shown that:

- The onset of vortex breakdown at the trailing edge of the wing is only weakly influenced by the free stream Mach number for the present Mach number range ($M_\infty \leq 0.8$ ) wich is in agreement with recent experimental observations[27].

- The upstream progression of the vortex bursting with incidence is faster for supersonic than subsonic core flows, even for flows free of shock waves.

- The fast upstream shifting of the vortex breakdown is reponsable of the strong degradation of the aerodynamics performances of a delta wing in transonic flow.

- Terminating or rear shocks develops after vortex bursting.

- A convergent-divergent channel is formed between the wing surface and the vortex axis which accelerates the subsonic flow to supersonic speeds. Crossflow shocks may be formed within the channel already for free stream Mach numbers with a normal component to the wing leading edge $M_N \approx 0.4$ .

- As the velocity in the channel becomes supersonic, the induced suction peak of pressure on the wing surface underneath the leading edge vortex is reduced.

- The channel introduces strong radial velocities within the vortex core which leads to a non-uniform distribution of total velocity inside the vortex core.

- The vortex core deforms and has a rather flat shape due to the different magnitude of the centrifugal forces acting on top and bottom of the core.

- The core deformation is the main source of vorticity production within the vortex core.

- The missaligment between vorticity and velocity vectors leads to entropy gradients which are the main source of the losses of total pressure found within a core flow of a leading edge vortex of a delta wing.

## References

1. Hoeijmakers H.W.M.: Modeling and Numerical Simulation of Vortex Flow in Aerodynamics. AGARD CP-494, paper No.1(1990), 1-1 to 1-46.

2. Newsome R.W. and Kandil O.A.: Vortical Flow Aerodynamics -Physical and Numerical Simulation- AIAA paper 87-0206(1987).

3. Elsenaar, A.; Bütefisch, K.; Hjelmber, L. and Bannink W.J.: The International Vortex Flow Expenment. AGARD CP-437(1988), 9-1 to 9-23.

4. Erickson, G.E.; Schreiner, J.A. and Rogers, L.W.: On The Structure, Interaction and Breakdown Characteristics of Slender Wing Vortices at Subsonic, Transonic and Supersonic Speeds. AIAA paper 89-3345 (1989).

5. Mc Millin, S.N.; Thomas, J.L. and Murman, E.: Navier-Stokes and Euler Solutions for Lee-Side Flows Over Supersonic Delta Wings - A Correlation With Experiments. NASA Technical Paper 3035(1990).

6. Longo, J.M.A.: Simulation of Complex Inviscid and Viscous Vortex Flows. IUTAM Symposium on Fluid Dynamics of High Angle of Attack(1992), Japan.

7. Murman E. and Rizzi A.: Application of Euler Equa-

tions to Sharp Edge Delta Wings With Leading Edge Vortices. AGARD CP-412(1986), 15-1 to 15-13.

8. Hitzel, S.: Wing Vortex-Flows Up into Vortex-Break-down - A Numerical Simulation. AIAA paper 88-2518(1988).

9. O'Neil, P.J.; Barnett, R.M. and Louise C.M.: Numerical Simulation of Leading-edge Vortex Breakdown Using an Euler Code. AIAA paper 89-2189(1989).

10. Longo, J.M.A.: The Role of The Numerical Dissipation on The Computational Euler Equations Solutions for Vortical Flows. AIAA paper 89-2232(1989).

11. Raj, P.; Sikora, J.S and Keen, J.M.: Free-Vortex Flow Simulation Using a Three-dimensional Euler Aero-dynamicMethod. ICAS Proceedings(1990), 604-616.

12. Longo, J.M.A. and Das A.: Numerical Simulation of Vortical Flows over Close-Coupled Canard-Wing Configuration. AIAA paper 90-3003(1990).

13. Hoeijmakers, H.W.; Jacobs, J.M.J.W. and Van den Berg J.I.: Numerical Simulation of Vortical Flows over a Delta Wing at Subsonic and Transonic Speeds. ICAS Proceedings(1990).

14. Agrawall, S.; Barnett R.M. and Robinson, B.A.: Investigation of Vortex Breakdown On a Delta Wing Using Euler and Navier-Stokes Equations. AGARD CP-494(1990), 24-1 to 24-12.

15. Malfa, E.; Guarino, L. and Visintini L.: Application of Euler Equations To The Computation of Vortex Flows on Wing-Body and Close-Coupled Wing-Body-Canard Configurations. AIAA paper 91-3306(1991).

16. Longo, J.M.A.: Numerische Analyse der Strömungs-felder von Deltaflügelkonfigurationen ohne und mit Canard. Zentrum für Luft und Raumfahrttechnik, TU Braunschweig, ZLR-Forschungsbericht 93-09(1993).

17. Radespiel, R.: A Cell-Vertex Multigrid Method for the Navier-Stokes Equations. NASA TM-101557(1989).

18. Atkins, H.: A Multi-Block Multigrid Method for the Solution of the Euler and Navier-Stokes Equations. AIAA 91-0101(1991).

19. Rossow, C.C.: Efficient Computation of Inviscid Flow Fields Around Complex Configurations Using a Multi-Block Multigrid Method. Fifth Copper Mountain Conference on Multigrid Methods, Colorado, USA(1991).

20. Jameson, A., Schmidt, W.and Turkel, E.: Numerical Solutions of the Euler Equations by Finite Volume Methods Using Runge-Kutta Time Stepping Schemes. AIAA paper 81-1259(1981).

21. Kommallein, S.: Untersuchungen über die Wirbel-struktur an einem schlanken Flügel bei großen Anstellwinkeln. Zentrum für Luft und Raumfahrt-technik, TU Braunschweig, ZLR-Forschungsbericht 93-07(1993).

22. Wendt, J.F.: Compressibility Effects On Flows Around Simple Components. AGARD LS-121(1982), 7-1 to 7-20.

23. Narayan K.Y. and Seshadri S.N.: Vortical Flows on the Lee Surface of Delta Wings. IUTAM Symposium Transsonicum III(1988), 329-338.

24. Batchelor, G.K.: Axial Flow in Trailing Line Vortices. J.Fluid Mech. 20(1964), 645-658.

25. Oelker, H.-Chr.: Aerodynamische Untersuchungen an kurzgekoppelten Entenkonfigurationen bei symme-trischer Anströmung. Zentrum für Luft und Raum-fahrttechnik, TU Braunschweig, ZLR-For schungsbericht 90-01(1990).

26. Das, A.: Analysis of Spiraling Vortical Flows around Slender Delta Wings Moving in an Inviscid Medium. ZAMM. Z. angew. Math. Mech. 71(1991), 11, 465-471.

27. Elsenaar, A. and Hoeijmakers, H.W.M.: An Experimental Study of The Flow over a Sharp-edge Delta Wing At Subsonic and Transonic Speeds. AGARD CP-494(1990), 15-1 to 15-19.